ORIGINAL ARTICLE

Effect of Co and Fe contents on the microstructure and corrosion behaviour of heat-treated Ni-Fe-Co superalloys in 3.5 wt% NaCl aqueous solution

Itshepeng Mogaleadi Christinah Bopape[1] · Enoch Nifise Ogunmuyiwa[2] · Mxolisi Brendon Shongwe[1] · Nthape Percyval Mphasha[3] · Nthabiseng Ntholeng[1]

Abstract

The effect of chemical composition on the corrosion behaviour of heat-treated Ni-Fe-Co superalloys has been investigated in aerated 3.5 wt% NaCl aqueous solution. Nickel-base alloys with varying amounts of Fe (5–20 wt%) and Co (30–45 wt%) were fabricated via spark plasma sintering. The alloys were heat-treated at 1000 °C in a muffle furnace for 1 hour, and then quenched in distilled water for 5 minutes. Corrosion resistance of the alloys was analysed by measuring potentiodynamic polarization. Corrosion parameters, i.e. E_{corr}, i_{corr}, E_{pass} and i_{pass}, were compared for different Co and Fe contents to establish a relationship between the alloy composition and corrosion properties. The results showed that the corrosion resistance of the alloys improved with increasing Co and decreasing Fe content. Accordingly, corrosion rate and corrosion current density (i_{corr}) decreased with increasing Co content and the imposition of heat treatment. Ni-5Fe-45Co (wt%) showed the highest resistance to corrosion with corrosion rates of 0.0145 and 0.00294 mm/year in as-sintered and heat-treated conditions, respectively. Generally, heat treatment improved the grain homogeneity of the microstructures. Characterisation of surface morphologies of as-sintered and heat-treated corroded alloys was conducted using X-ray diffraction (XRD) and scanning electron microscopy (SEM) equipped with energy-dispersive spectroscopy (EDS).

Keywords Heat treatment · Ni-base superalloy · Corrosion resistance · Microstructure

1 Introduction

Ni-based superalloys are an unusual class of metallic materials widely used in aircraft engines, power-generation turbines, rocket engines owing to their exceptional combination of good high-temperature corrosion and mechanical properties [1]. The good high-temperature performance of these alloys is predominantly influenced by two phases: a disordered solid-solution face centered cubic (fcc) γ matrix and $\gamma\prime$ precipitates with a coherent, ordered $L1_2$ crystal structure embedded within the γ matrix. This means that $\gamma\prime$ precipitates have a strengthening effect on the alloys, with the amount and distribution of precipitates playing a critical role. Hence, a good combination of mechanical and corrosion properties is reliant on the microstructure of the alloy, i.e. primarily on the chemical composition, volume fraction and morphology of $\gamma\prime$ particles [2].

Considering the highly corrosive environments that Ni-based superalloys are typically used under, appreciable attention has been given to the effects of alloying elements on their corrosion behaviour in chloride-ion containing environments [3]. The effects of alloying elements such as cobalt (Co), chromium (Cr), iron (Fe), molybdenum (Mo) and tungsten (W) on the corrosion behaviour of Ni-based superalloys have been investigated [4–6]. Among all the elements investigated, Co has been considered to be critically strategic to Ni-based superalloys because it provides solid solution strengthening to the microstructure. Zhao et al.

✉ Nthabiseng Ntholeng
sthabi@gmail.com

1   Department of Chemical, Metallurgical and Materials Engineering, Tshwane University of Technology, Pretoria, 0001, South Africa

2   Department of Chemical, Materials and Metallurgical Engineering, Botswana International University of Science and Technology, Palapye, Botswana

3   School of Chemical and Metallurgical Engineering, University of the Witwatersrand, Johannesburg, South Africa

[5] investigated the hot corrosion behaviour of INCONEL 740 and suggested that decreasing the Co content to below 20 wt% provides better corrosion resistance. Lu et al. [6] studied the effect of Co content on the oxidation and corrosion of Ni-Fe superalloys by varying Co content between 6 and 20 wt%, and concluded that samples with high Co content offered good oxidation resistance by forming a protective film of Cr_2O_3. However, this layer of film could not prohibit the inward diffusion of sulphur thus offering minimal improvement in corrosion resistance. Essentially, the films should serve as an effective barrier between the substrate materials and the corrosive environment [7–9], protecting them from additional corrosion processes. Hence, there seem to be a need to study Ni-based superalloys with much higher Co contents.

Although the nickel-based superalloys are resistant to pitting attack in chloride environments, passivity breakdown may occur resulting in the premature microstructural degradation and mechanical failure [3]. Hence, other solid solution strengtheners, in both γ and γ' precipitates, such as cobalt (Co), iron (Fe), titanium (Ti) and vanadium (V) can be explored to enhance the corrosion properties of the alloys [10]. Aba-Perea et al. [11] found that there was a high percentage of disordered solid solution elements including Cr, Mo and Co in the γ phase with a continuous matrix of fcc phase. These alloys were found to give better mechanical and corrosion properties when compared to other Ni-based alloys, even at higher temperatures.

Whilst Ni-based superalloys containing Fe and Co may have good corrosion properties, heat treatment may be employed to enhance these properties through homogenisation of the microstructures [12]. Conventional heat treatment processes can be carried out in either two or three steps: solution treatment followed by a single or double step aging treatment. During these heat treatment processes, the γ' precipitates are respectively refined and dissolved and thus strengthening the γ' matrix [12]. Solid solution heat treatment in Ni-base superalloys is intended to obtain moderate grain size and dissolve the precipitating phase for subsequent re-precipitation in an optimized morphology and size. Then, single or double steps of aging treatments, helps to achieve controlled γ' re-precipitation and M23C6 typed carbides growth at grain boundaries [13, 14]. Balikci et al. [15] proposed two mechanisms for growth of γ' precipitates: coalescence of the small particles to the larger ones and extraction of dissolved elements from the saturated solid solution matrix to the precipitates. Hence, high aging temperatures would be used for the formation of large carbides and γ' particles, while lots of fine γ' particles are formed during the low temperature aging [13, 14]. Pike et al. [14] showed that conventional heat treatment can result in the formation of fine, spherical γ' precipitates and discrete grain particles. Essentially, the solution temperature

and the aging time can be tailored to control the grain size of γ' precipitates [16]. For example, Zhao et al. [12] showed that the microstructure of a Ni-Fe-based superalloy heat-treated in the temperature range of 700–1150 °C for 1 hour had coarse γ' precipitates at temperatures between 780 °C and 810 °C. With further increase in temperature to 900 °C and above, the γ' precipitates became coarser suggesting a reduced volume fraction of $\gamma + \gamma'$ eutectic phases. Despite these investigations, there are however no studies in literature on the effect of heat treatment on the corrosion properties of Ni-Fe-Co superalloys. Hence, the influence of heat treatment on the morphology of Ni-Fe-Co superalloys and its subsequent impact on corrosion properties is worth studying.

In this study, the microstructure-corrosion property relationship of Ni-Fe-Co superalloys was investigated to establish the effects of chemical composition and heat treatment on the electrochemical corrosion behaviour of Ni-Fe-Co superalloys in a 3.5 wt% NaCl solution. Passivity mechanisms and the evolution from localised pitting corrosion to general corrosion with heat treatment were revealed by studying the electrochemical corrosion process behaviour. The influence of chemical composition on the electrochemical behaviours of the alloys was discussed to indicate the growth process and failure mechanism of the passive films. Thereafter, the relationship between heat treatment and corrosion resistance properties was outlined.

2 Experimental procedure

2.1 Mixing and milling of raw powders

Commercial powders of Ni, Fe, and Co with particle sizes of ≥ 0.5 to 30, ≤ 44, and ≤ 44 μm, respectively, were provided by WEAR TECH (Pty) Ltd. For particle size reduction, the powders were processed individually in a high-energy planetary ball mill with steel balls and vials as grinding media. Milling was done for 15 h at a vial rotation speed of 350 rpm and ball to powder ratio of 10:1. Wet milling with ethanol as the suspension media was used to prevent particle agglomeration. Milled powders, of varying compositions as shown in Table 1, were then mixed in a tubular mixer for 6 hours at a speed of 49 rpm.

2.2 Sintering of admixed powders

SPS machine was used to produce the sintered alloys. The sintered alloys were manufactured by placing an equal amount of mixed powders in graphite die with an internal diameter of 20 mm. To eliminate contamination and make it easier to remove the sample after sintering, graphite foil was inserted inside the die. The mixed powder samples

Table 1 Chemical composition of the sintered Ni-Fe-Co alloys

	Nickel (Ni)	Iron (Fe)	Cobalt (Co)
Sample		Wt%	
1	50	20	30
2	50	15	35
3	50	10	40
4	50	5	45

were sintered at a temperature of 900 °C, heating rate of 150 °C/min, holding time of 10 min and pressure of 50 MPa. Post the sintering process, the samples were sandblasted and their density was measured using the Archimedes principle.

2.3 Heat treatment

For heat treatment tests, the specimens were cut to a diameter of 13 mm and a thickness of 170 mm. The specimens were heat-treated for 1 hour at 1000 °C in a muffle furnace, and then quenched in distilled water for 5 min and cooled to room temperature.

Specimen dimensions similar to those used in heat treatment tests were used for electrochemical corrosion tests. The surfaces of the specimens were ground and polished to a mirror surface finish with a 1.0 µm alumina (Al_2O_3) polishing paste. Prior to the heat-treatment and electrochemical tests, specimens were rinsed with deionised water and ethanol, and then dried in a drying oven.

2.4 Electrochemical measurements

Electrochemical tests were conducted using a standard three-electrode system in naturally aerated 3.5 wt% NaCl aqueous solution prepared with deionised water. A temperature of 30 ±1°C for an hour and a scan rate of 1.27 mV/s were used. The three-electrode system contained a saturated calomel electrode (SCE) reference electrode, a platinum counter electrode, and the alloy sample as the working electrode. Potentiodynamic polarization tests were conducted using an Autolab potentiostat interfaced with a computer for data acquisition and analysis, and the Tafel extrapolation method was used to estimate the potential and corrosion rates.

2.5 Characterization of sintered specimens

Microstructures of the sintered and corroded specimens were examined using scanning electron microscopy (SEM) equipped with energy-dispersive X-ray spectroscopy (EDS). As-sintered and heat-treated samples were cut, ground, mounted and polished for metallographic examination. Morphological studies were conducted using SEM and EDS.

# 3 Results and discussion

3.1 Powder analysis

Owing to the fact that Fe powder particles are spherical and non-porous, and Ni and Co particles have irregular shapes and agglomerates, the milled admixed powders have sheet-like morphology (Fig. 1). This change in particle morphology could be attributed to the high force impact of ball-ball and ball-wall collisions during milling [17]. The flatness of the particles is due to the extreme plastic deformation experienced during the milling of the powders over long periods of time. According to Karimbeigi et al. [18] and Rominiyi et al. [19], long milling periods can cause particle disintegration, which result in fracture and welding cycles triggered by strain hardening of the materials. This was observed in this study when the admixed powder particles would collide with each other, thus bonding together to form flaky particles seen in Fig. 1. It can then be expected that the resultant microstructures would have lamellar structures due to the prior bonding of the particles.

Figure 2 shows the X-ray diffraction patterns of the admixed powders of different compositions. The presence of C, Co, Fe and Ni is detected in all the admixed powders. The detected C could be attributed to the carbon released into the milled powders during the stainless steel ball-ball and ball-vial wall interactions during the milling process. With the decrease in Fe and increase in Co contents of the alloys, the peaks at 65° and 82° (2θ) become less pronounced with complete disappearance for Ni-5Fe-45Co (wt.%). No other phases could be detected, indicating that there was no reaction during the milling operations. However, traces of Cr were detected by EDS (Fig. 3), which could be from the addition of Co which contained minute amounts of Cr.

3.2 Microstructure analysis

The sintered alloy discs were cut and ground. A collimated beam of X-ray (Cu- Kα, λ = 1.5406 Å) was incident onto the cross-section of the alloy material. Phase analysis (Fig. 4) of the sintered alloys shows five characteristic peaks similar to the admixed powders except for the Ni-5Fe-45Co alloy in which four peaks could be detected. The formation of new phases is evident in the sintered alloys which indicates that elemental diffusion occurred during the sintering process. The formation of (γ')-FeNi$_3$ and γ-(NiFe) phase is evident in both low and high angles (2θ). Both (γ')-FeNi$_3$ and γ-(NiFe) phases are detected in the same peaks which is indicative of coherent precipitation of both phases [3]. The (γ')-FeNi$_3$ is the primary strengthening phase typical in nickel-base superalloys [20]. It has been reported that the γ' precipitates increase the toughness of the alloys due to their structural coherence with the matrix [21–23], which may be
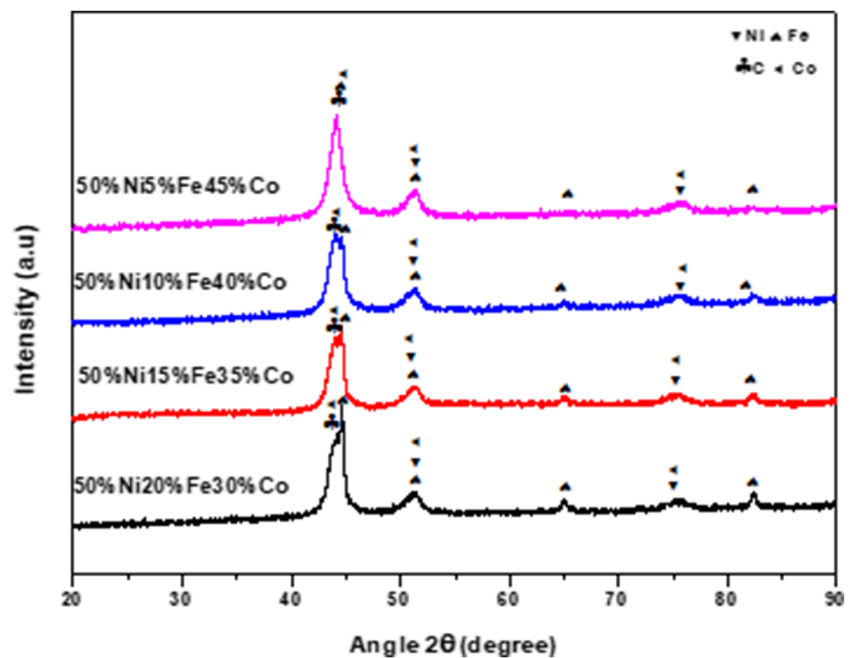
Fig. 1 SEM analysis of admixed powder of (a) Ni-20Fe-30Co, (b) Ni-15Fe-35Co, (c) Ni-10Fe-40Co and (d) Ni-5Fe-45Co
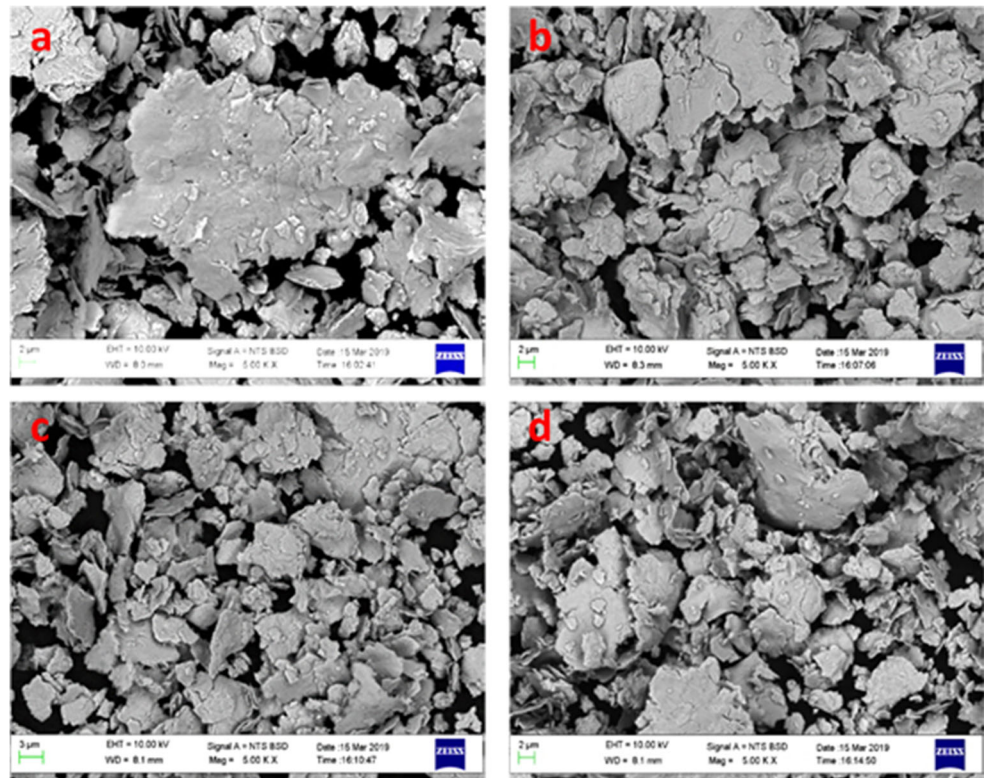

related to their corrosion resistance. The additional phases observed were: Co-Fe (bcc) and an orthorhombic Fe_3C. Formation of Fe_3C shows that a sintering temperature of 900 °C allowed for diffusion of C impurities. The formation of (Fe,Ni) phase was also observed by Turchanin et al. [24], which is indicative of unreacted metal particles suggesting that there may be particle segregation.

Metallography analysis of the sintered alloys was carried on the polished surface of the samples and SEM micrographs are presented in Fig. 5. The surface analysis of the sintered alloys showed lamellar microstructure with formation of pores. The observed pores appear to vary in size with some interconnected. Formation of pores is indicative of poor particle bonding which is in agreement

**Fig. 2** Diffraction patterns of admixed powders with various Fe and Co contents

Fig. 3 EDS analysis of admixed powder of (a) Ni-20Fe-30Co, (b) Ni-15Fe-35Co, (c) Ni-10Fe-40Co and (d) Ni-5Fe-45Co
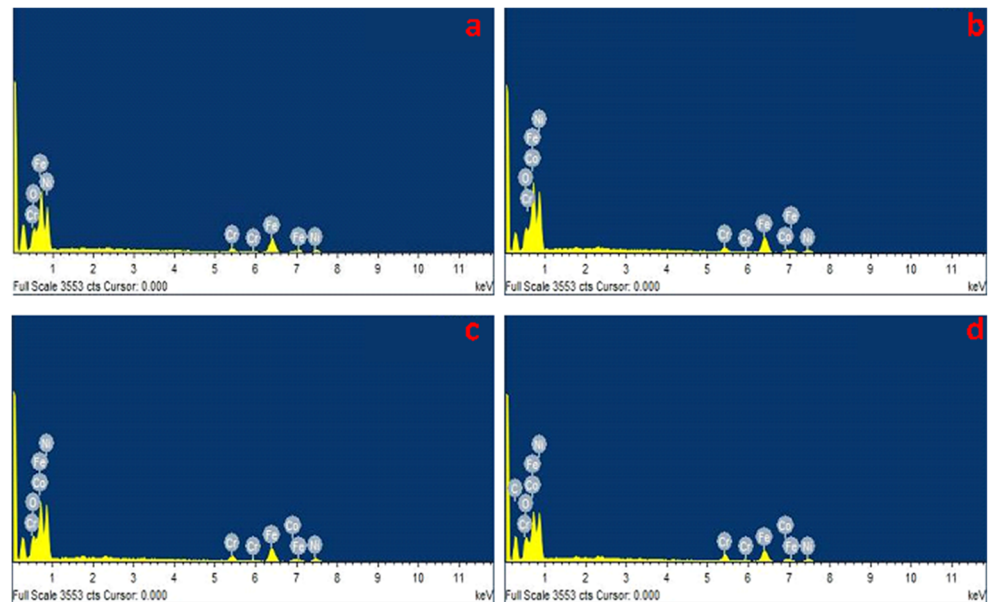

with the detected metal phases by XRD (Fig. 4) which could be due to particle segregation or poor particle diffusion. The observed near-lamellar structure is the precipitated γ' phases (indicated by white arrows on the insert Fig. 5b) interconnected by narrow channels γ phase at the interface (shown by red arrows in insert Fig. 5b).This further depicts that both γ' phase and γ phase are coherently precipitated which explains why both phases could be seen in the same peaks (Fig. 4). Contrary to our findings, Long et al. [25] reported the formation of cuboid γ' phases with narrow channels of γ phase between the cuboids. Reed et al.

[26] further elucidated that microstructure evolution of the Ni-based superalloys was dependent on various factors, including the cooling rate, the applied heat treatments, solution annealing and aging. Other researchers reported that the formation of cuboids morphology in Ni-based superalloys evolves from the dendritic shape γ' phase [27]. Therefore, the formation of lamellar microstructure in this study can be attributed to rapid cooling during sintering. The distinctive dark and light grey spots on the surface were shown to be Ni-Co rich phases by EDS (Fig. 6).

Fig. 4 Diffraction patterns of the as-sintered ternary alloys at 900 °C with various Fe and Co content
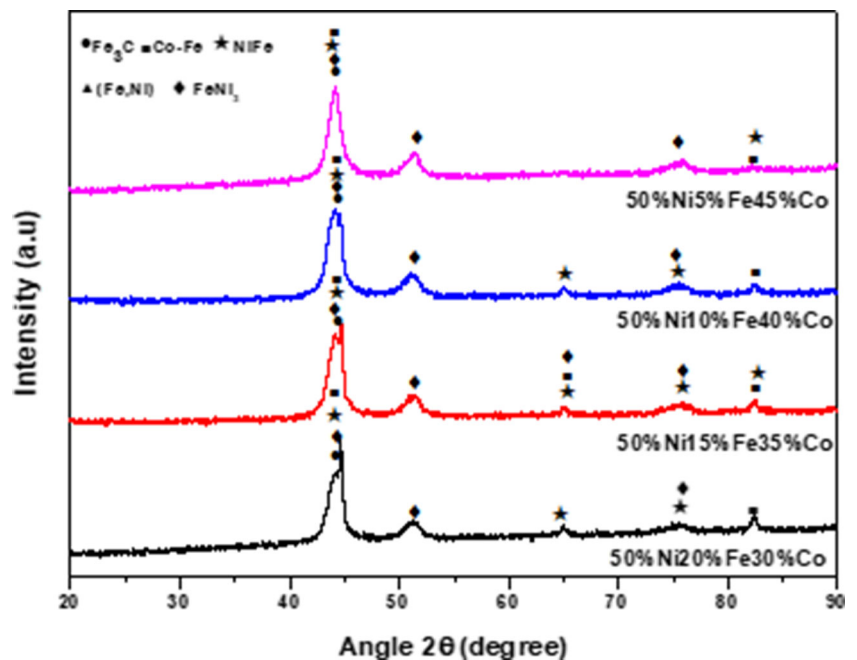
**Fig. 5** Sintered alloys of (a) Ni-20Fe-30Co, (b) Ni-15Fe-35Co, (c) Ni-10Fe-40Co and (d) Ni-5Fe-45Co
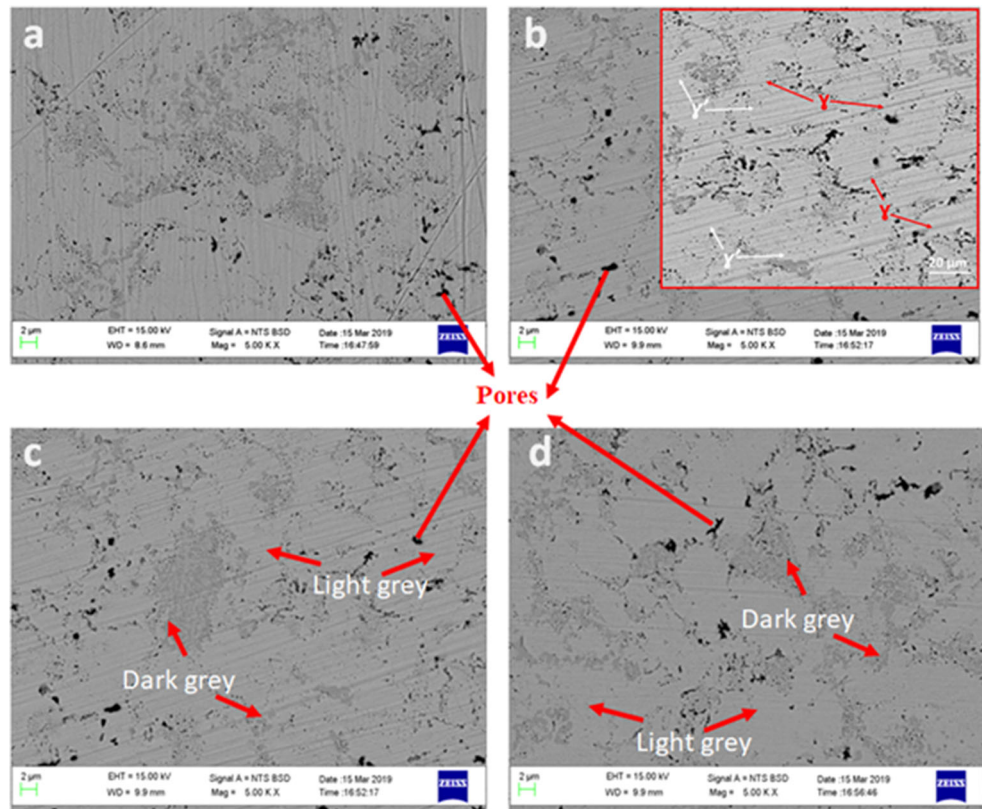
3.3 Effect of heat treatment on microstructure

A key factor in the application of super alloys is the microstructural properties which are greatly influenced by heat-treatments [12]. It has been shown that heat treatment affects both grain size and precipitates distribution which have a great impact on mechanical properties [28]. Moreover, heat treatments are recommended for nickel-base superalloys as

it helps to achieve the high volume fraction, better size distribution of $\gamma\prime$ precipitates and carbides [12]. The volume percentage and particle size of the precipitated $\gamma\prime$ are linked to the hardness of the alloys. The hardness of the alloy increases with particle size growth while high temperature strength increases with the amount of the phase present [29]. The sintered alloys were heat-treated at 1000 °C for 1 h in a muffle furnace and thereafter quenched in distilled water.

Fig. 6 Sintered alloys of (a) Ni-20Fe-30Co, (b) Ni-15Fe-35Co, (c) Ni-10Fe-40Co and (d) Ni-5Fe-45Co
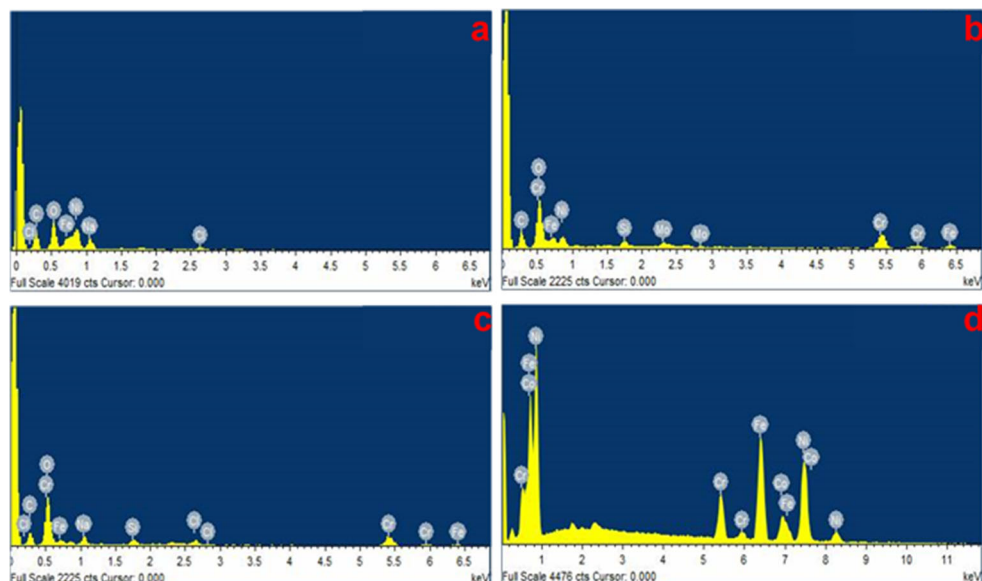
Microstructure of the heat-treated samples is presented in Fig. 7. The heat-treated samples appear more homogenous compared to the sintered samples. This suggests that the microstructure of the alloys have been improved by heat treatment. A significant decrease in porosity is also evident suggesting that there is enhanced particle bonding. On the contrary, there is precipitate coarsening observed in samples with high Fe content and low Co content (Fig. 7a and b) suggesting the presence of an undissolved $\gamma\prime$ phase.

Zhao and colleagues [12] reported coarsening in $\gamma\prime$ phase in Ni-based superalloy during thermal exposure at 810 °C and 840 °C. It was further concluded that higher aging temperatures (810 °C and 840 °C) depressed the nucleation of $\gamma\prime$ particles, which also provided additional degradation of precipitation hardening. Alloys with high Co content (Fig. 7c and d) appear to be more homogenous with refined grain distribution than those with low Co content (Fig. 7a and b). This indicates that the precipitated $\gamma\prime$ phase has dissolved into the matrix. Dissolution of $\gamma\prime$ precipitates suggest that Co (low melting temperature 1132 °C) may have reached a molten state promoting the diffusion of precipitated phases, while in low Co content alloys formation of

molten Co could have been minute to prevent particle segregation hence coarse islands visible on the microstructure. Furthermore, the homogenous distribution of refined grains in Fig. 7c and d are indicative of improved particle bonding thus better mechanical properties.

Elemental analysis showed traces of impurities of Mo, Cr and Si on alloys with low Co content (Fig. 8a and b) while alloys with high Co content (Fig. 8c and d) showed no traces of impurities except C. The absence of impurities in high Co concentration alloys could indicate that Co reached a molten state during heat treatment at 1000 °C, allowing impurities and precipitated phases to diffuse. As a result, for low Co concentration alloys, the creation of liquid Co was insufficient to induce high impurity diffusion.

To further understand the effects of heat treatment on sintered alloys, a crystal structure study was performed. In comparison to sintered alloys, heat-treated alloys appear to have sharper and higher intensities. This could be due to the occurrence of grain refinement within the heat-treated alloys' matrix. Figure 9 shows that there is a gradual shift in diffraction pattern from low to high diffraction angles with decreasing Co and increasing Fe contents, respectively. This signifies a change in unit cell volume, implying that the

Fig. 7 Heat-treated alloys of (a) Ni-20Fe-30Co, (b) Ni-15Fe-35Co, (c) Ni-10Fe-40Co and (d) Ni-5Fe-45Co
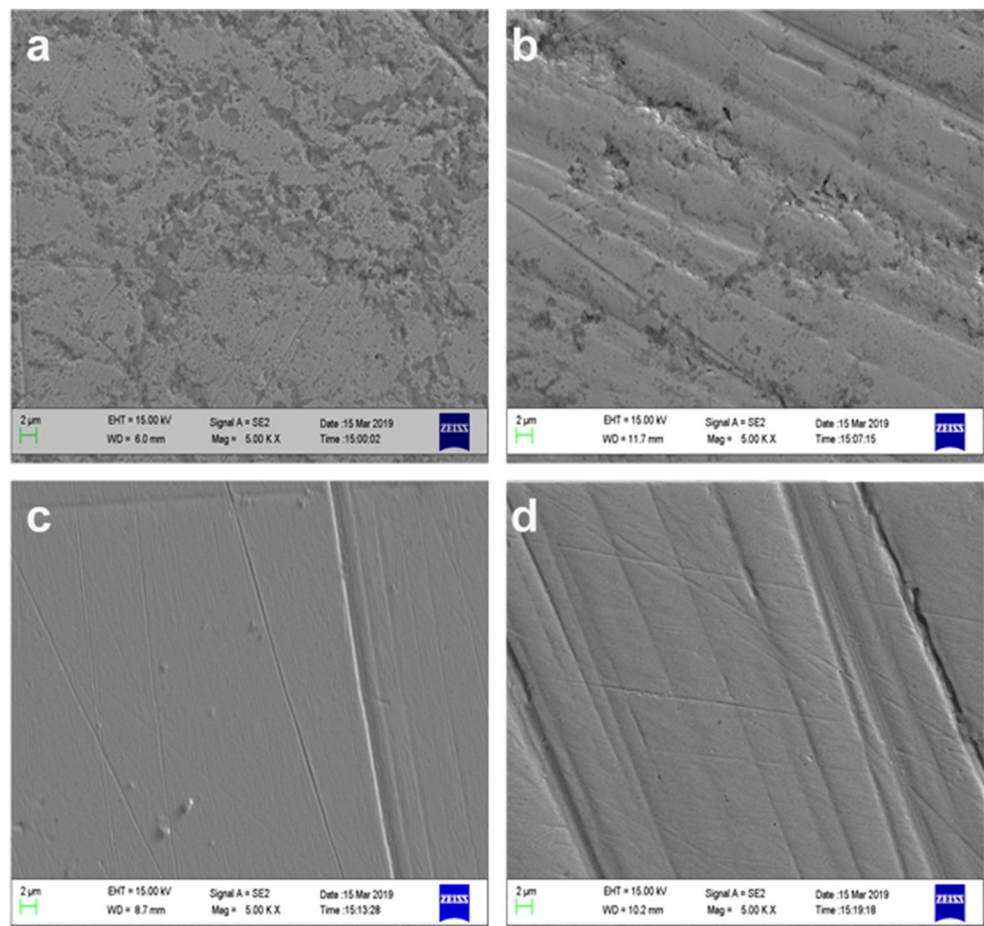
Fig. 8 Heat-treated alloys of (a) Ni-20Fe-30Co, (b) Ni-15Fe-35Co, (c) Ni-10Fe-40Co and (d) Ni-5Fe-45Co
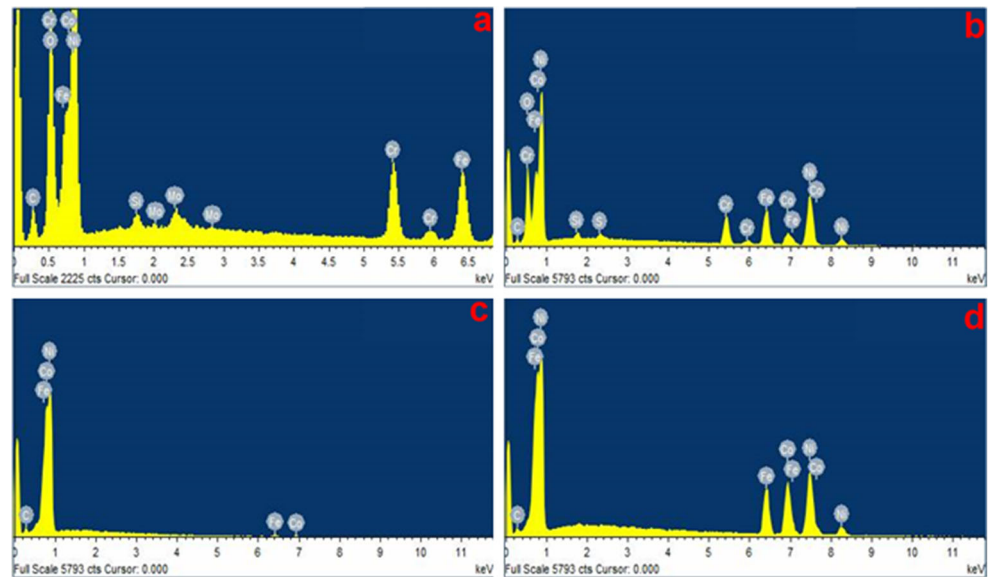
volume of the unit cell has increased. Berthod et al. [30] reported that during solid solution strengthening, alloying elements with heavy atoms can cause local matrix crystalline network distortion. The same is observed in this study as supported by the formation of $\gamma\prime$ precipitates at lower Co contents. Furthermore, the alloys with the low Co content (Ni-20Fe-30Co and Ni-15Fe-35Co) show two low intensity peaks at 30° and 36° which correspond to orthorhombic Fe_3C and γ-(Ni, Fe), respectively. And, two more peaks at 57° and 63° correspond to similar phases including a Co-Fe (bcc) phase which could not be detected on alloys with high

Co content. This could be attributed to the dissolution of low temperature intermetallics such as CoFe and ($\gamma\prime$)-$FeNi_3$ into the matrix which may occur due to heat treatment at 1000 °C, as observed by Turchanin et al. [24]. This finding further supports the idea that alloys with a high Co content produce enough molten Co to allow precipitated phases or intermetallics to diffuse into the matrix. This is further supported by the homogeneous grain refinement seen in the microstructures of Ni-10Fe-40Co (Fig. 7c) and Ni-05Fe-45Co (Fig. 7d), which revealed no coarse island development. In contrast to low Co alloys, three different

Fig. 9 Diffraction patterns of Heat-treated alloys with various Fe and Co content
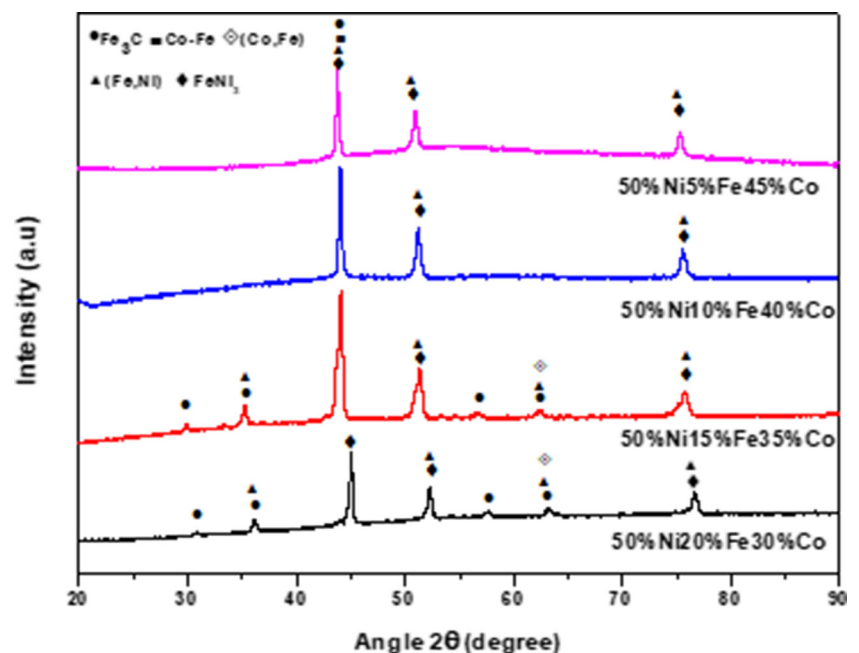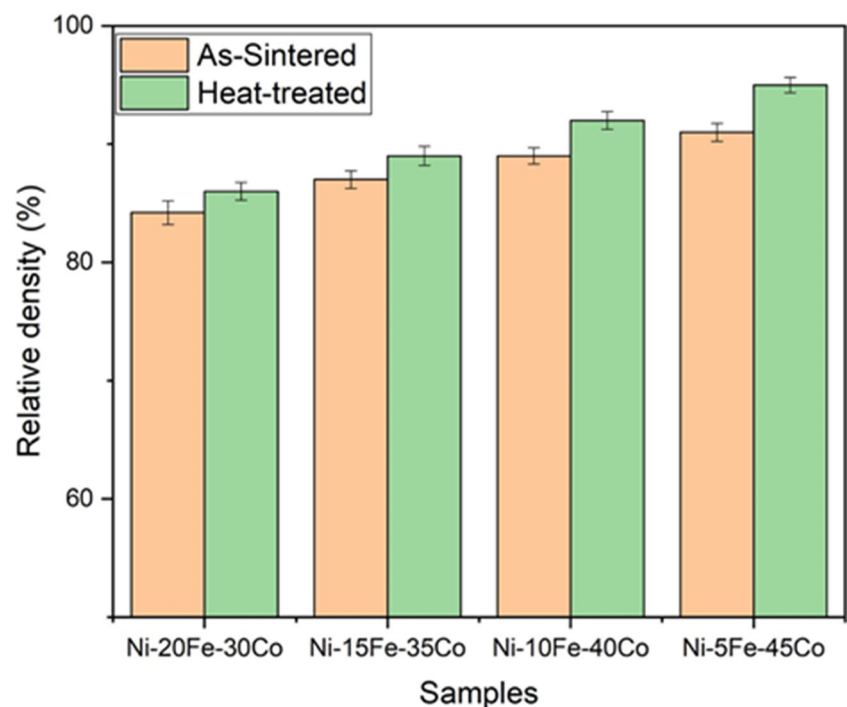
peaks have been identified for Ni-10Fe-40Co and Ni-05Fe-45Co, leading to the creation of Ni2.76Fe1.13Co0.11 (PDF#:96-900-0089). This is consistent with the EDS data in Fig. 8, which indicated no impurity formation.

3.4 Relative density

Figure 10 shows the density values of sintered and heat-treated alloys, where the calculated, theoretical and relative density values are compared. The density of the alloys was shown to have a direct relationship with the composition variation. Density values of the alloys increase with an increase in Co content and a decrease in Fe content. This could be attributed to the lower melting point of Co (1132 °C), which implies that a portion of the Co is already molten, enhancing the partial liquid phase sintering of the alloys.

When compared to sintered alloys, heat-treated alloys have a higher relative density which can be attributed to improved particle diffusion. Other researchers established that the particle size of the $\gamma\prime$ precipitates also affects the strength of alloys. As a result, higher alloy hardness is achieved as the particle size of the $\gamma\prime$ phase increases [20]. Zhong et al. [13] reported that high temperature treatment are used to produce large size of $\gamma\prime$ particles, while low temperature aging results in the formation of lots of fine $\gamma\prime$ particles. Microstructure of the heat-treated alloys (Fig. 7) shows a high volume percentage of $\gamma\prime$ precipitates compared to the γ phase. Therefore, greater relative density in heat-treated alloys could be attributed to increased volume and improved size of $\gamma\prime$ precipitates.

3.5 Electrochemical behaviour

Electrochemical studies were carried out in a 3.5% NaCl solution with a scan rate of 1.27 mV for 3600 s on both sintered and heat-treated alloys. The results of polarizations such as corrosion current density (I_{corr}), corrosion potential (E_{corr}), corrosion rate (CR), and polarization potential (RP) were obtained using the Tafel extrapolation. The obtained corrosion measurements of both the as-sintered and heat-treated alloys are shown in Tables 2 and 3. In contrast to sintered alloys, heat-treated alloys have a lower corrosion resistance. As a result, it can be concluded that heat treatment improved microstructure properties of the sintered alloys. High corrosion rate in sintered alloys can be attributed to poor particle bonding as well as the presence of impurities. Dutta et al. [31] reported that localised corrosion diminishes in the absence of common structural defects such as the grain boundaries, dislocations and segregations. Hence, heat-treated alloys showed good resistance to corrosion due their more compact structure and good dissolution of precipitates. Therefore, the lack of passivation in sintered alloys could be driven by the presence of impurities which were detected by EDS. These impurities acted as catalysts for localised corrosion.

For both sintered and heat-treated alloys, the Ni-20Fe-30Co alloys had the highest corrosion rate of 0.28062 and 0.09941 mm/year, respectively. In contrast, Ni-5Fe-45Co recorded the lowest corrosion rates of 0.0145 and 0.00294 mm/year for as-sintered and heat-treated alloys, respectively. The brilliant corrosion resistance is primarily

Fig. 10 Relative density of the sintered and heat-treated alloys

Table 2 Polarization test results of as-sintered alloys

Alloy	ba (V/dec)	bc (V/dec)	E_{corr} calc (V)	i_{corr} (A/cm^2)	Corrosion rate (mm/year)	Polarization resistance (Ω)
Ni-20Fe-30Co	1.82E-01	3.86E-01	–0.91	2.57E-05	2.81E-01	2.09E+03
Ni-15Fe-35Co	1.87E-01	1.46E+00	–0.82	1.43E-05	1.56E-01	2.03E+03
Ni-10Fe-40Co	1.02E-01	1.89E-01	–0.92	1.09E-05	1.15E-01	2.64E+03
Ni-5Fe-45Co	7.04E-02	7.04E-01	–5.55	1.32E-06	1.45E-02	2.33E+03

due to the surface of Ni-base alloys covered by aqueous electrolytes. The substrate alloys are isolated by the film from the corrosive environment, which serves as a protective barrier and prevents further corrosion processes [28, 32]. Low corrosion rates may also be attributed to increasing Co content which becomes more efficient because of the excellent protective effectiveness of cobalt oxide [31, 32]. Solomon et al. [33] reported that alloying elements such as cobalt can significantly impact the effectiveness of chromium in forming or maintaining the passive film.

Ni-5Fe-40Co had a high corrosion rate of 0.03310 mm/year when compared to Ni-15Fe-35Co, which had a corrosion rate of 0.02301 mm/year. This is in contrast to SEM (Fig. 7b and c) results, which showed that Ni-5Fe-40Co had superior grain uniformity after heat treatment and a higher relative density than Ni-15Fe-35Co (Fig. 10). This indicates that the passive layer created did not provide complete protection for the substrate alloy, and the dissolution of the alloy continued. The absence of complete protection from passive film was attributed by El-Bagoury et al. [3] to an increase in potential, which caused the current to rise. This was expected given the presence of an aggressive anodic species, i.e. chlorides, in the corrosion solution. Linear polarization method was implemented to further understand how corrosion occurs at the surface of the alloys. Corrosion of both sintered and heat-treated alloys was studied in 3.5 wt% NaCl solution at 30±1°C for an hour. Polarization curves (Figs. 11 and 12) show the anodic and cathodic branch. Anodic branch represents alloy dissolution while hydrogen evolution is represented in the cathodic branch. The kinetics of anodic dissolution of Ni^{2+} ions in NaCl is governed by uniform dissolution following reaction path:

$$Ni \longrightarrow Ni^{2+} + 2e^- \tag{1}$$

Reduction reaction (reaction 2) takes place in the cathode, where H$^+$ ions are reduced to H$_2$ gas.

$$2H^+ + 2e^- \longrightarrow H_2 \tag{2}$$

The anodic domain can be divided into three distinct regions: active dissolution, passivation, and where the current density increases as potential increases. Sintered Ni-15Fe-35Co and Ni-5Fe-45Co have similar active-to-passive transition behaviour (Fig. 11), while sintered Ni-20Fe-30Co and Ni-10Fe-40Co have the same transition behaviour. Pitting can be observed above the passive region of both Ni-20Fe-30Co and Ni-10Fe-40Co (Fig. 11), which could be related to the breakdown of the passivation layer by chloride anions which occur at preferential surface sites (pores). This is mainly driven by the small changes in the passive-film structure and thickness [32]. The passive area of sintered Ni-20Fe-30Co appears to have narrower potential range than other sintered alloys, which Leffer et al. [34] attributed to the penetration and destruction of the passive film by chloride ions. Passive regions of Ni-15Fe-35Co and Ni-5Fe-45Co (Fig. 11) show wider potential range suggesting that the alloy surface is better passivated.

For the heat-treated alloys Ni-15Fe-35Co and Ni-20Fe-30Co, there is a small active to passive area (Fig. 12). Following the dissolution of Ni-20Fe-30Co, there is a decrease in current density and a minor increase in potential. This indicates that the alloy surface has pitting corrosion. The hump observed in the passive region of Ni-10Fe-40Co indicates that the passivation film has broken down, allowing more dissolved oxygen to reach the alloy surface. Further, after the passive region in Ni-10Fe-40Co, a minor drop in current density is seen, indicating that pitting may have happened. The corrosion rate of Ni-10Fe-40Co contradicts a study on amorphous alloys conducted by Angelini et al. [35] and Altube et al. [36], which found that increasing the Co

Table 3 Polarization test results of as-sintered alloys

Alloy	ba (V/dec)	bc (V/dec)	E_{corr} calc (V)	i_{corr} (A/cm^2)	Corrosion rate (mm/year)	Polarization resistance (Ω)
Ni-20Fe-30Co	6.86E-01	5.44E-01	–7,08E-01	9.09E-07	9.94E-02	1.45E+05
Ni-15Fe-35Co	4.06E-01	9.22E-01	–1.02E+00	2.11E-06	2.30E-02	5.80E+04
Ni-10Fe-40Co	2.06E-01	3.80E-02	–6.65E-02	3.02E-06	3.31E-02	4.62E+03
Ni-5Fe-45Co	1.69E-01	2.08E-01	–6.25E-01	2.72E-07	2.94E-03	1.49E+05

content resulted in satisfactory passivation. Solomon et al. [33], on the other hand, claim that the corrosion medium and concentration plays a role in the corrosion rate.

This is consistent with the findings in Table 3, which show corrosion rates of 0.02301 and 0.00294 mm/year for Ni-15Fe-35Co and Ni-5Fe-45Co, respectively. No pitting has been observed for Ni-15Fe-35Co and Ni-5Fe-45Co. Passive regions of both alloys appear to have a wide potential range, indicating that they are more resistant to corrosion attack. This is consistent with the results in Table 3, which show corrosion rates of 0.02301 and 0.00294 mm/year for Ni-15Fe-35Co and Ni-5Fe-45Co, respectively.

3.6 Morphology of corroded samples

Ni-based alloys are considered to have excellent resistance to corrosion, but are more likely to be vulnerable to cracking, pitting, and embrittlement of hydrogen [37]. The microstructure of the sintered and heat-treated alloys in 3.5 wt% NaCl solution is displayed in Figs. 13 and 14, respectively. Sintered alloys showed more corrosion on its alloys as compared to the heat-treated alloys.

It appears that general corrosion occurred on the surface of the sintered Ni-20Fe-30Co (Fig. 13a), Ni-15Fe-35Co (Fig. 13b) and Ni-10Fe-40Co (Fig. 14c) while corrosion
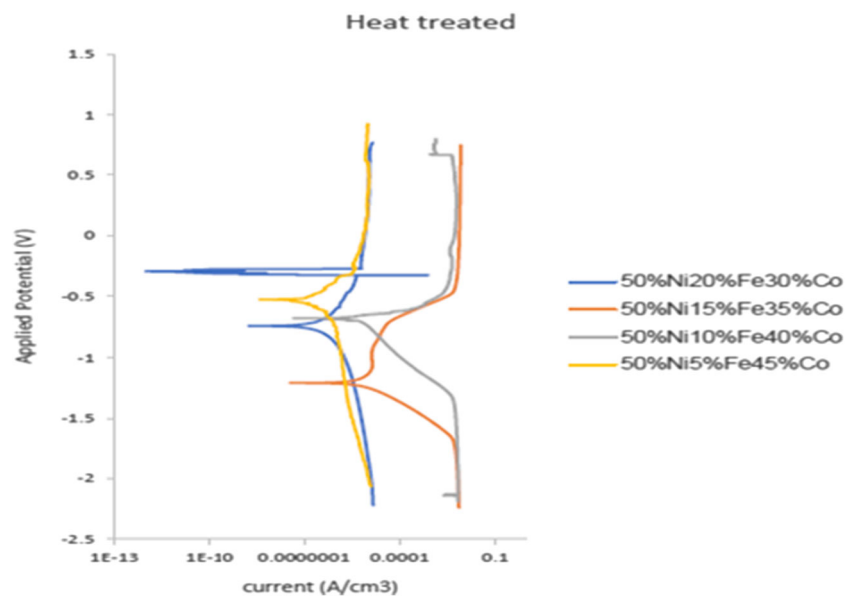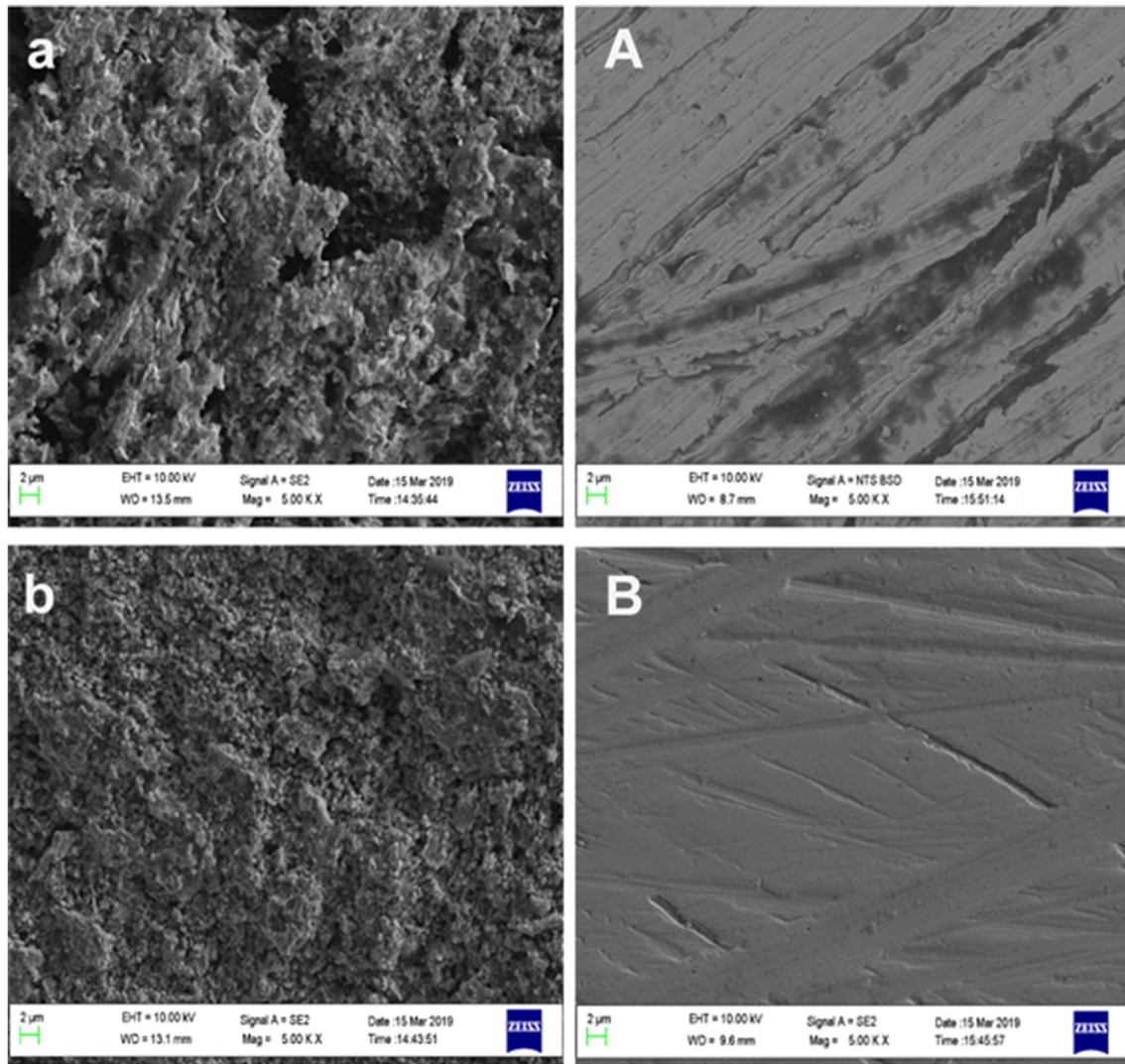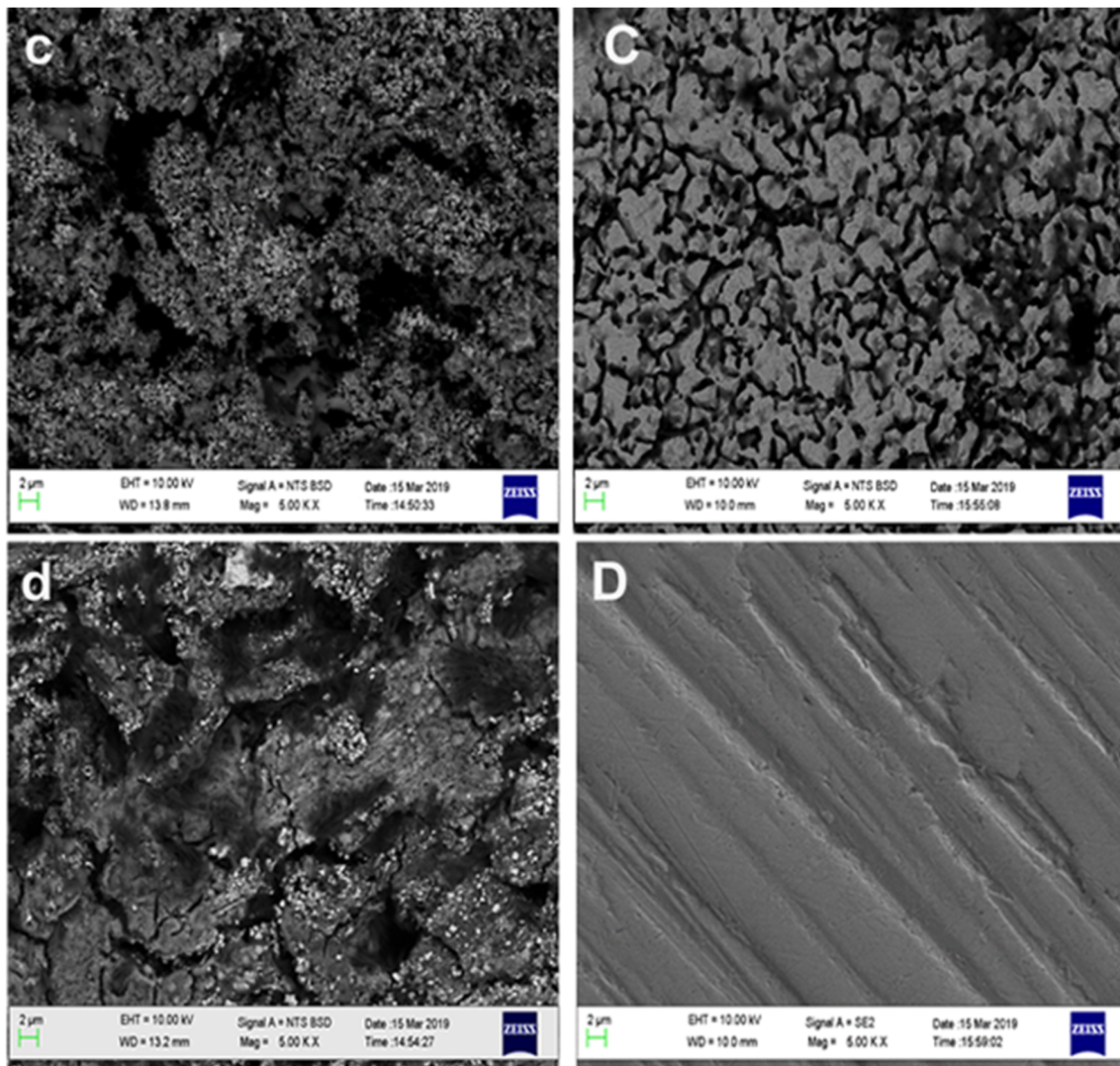
Fig. 13 SEM images of corroded sintered (a) Ni-20Fe-30Co and (b) Ni-15Fe-35Co, and corroded heat-treated (A) Ni-20Fe-30Co and (B) Ni-15Fe-35Co

products with visible cracks were observed on the surface of Ni-5Fe-45Co (Fig. 14d). Ibrahim et al. [38] reported that general corrosion is considered a uniform corrosion process in which numerous micro-corrosion cells are activated at the corroded site. Moreover, corrosion products do not form an effective barrier against further corrosion but allow reactants to penetrate to the substrate surface beneath and continue the corrosion cycle [34]. Similarly, Shongwe et al. [39] observed similar cracks when studying the corrosion behaviour of Ni50Fe40Co10. The formation of the cracks was associated with material loss that promoted deep corrosion penetration into the sample [39].

In comparison to Ni-15Fe-35Co (Fig. 13b) and Ni-5Fe-45Co (Fig. 14d), which show high corrosion rates, Ni-20Fe-30Co (Fig. 13a) and Ni-10Fe-40Co (Fig. 14c) show large and deeper corrosion pits. In the current

study, the formation of pores and particle segregation promoted deeper penetration of the reactants into the samples. On the contrary, Ni-10Fe-40Co sintered alloy showed a low corrosion rate of 0.1147 mm/year compared to Ni-15Fe-35Co with a high corrosion rate of 0.15636 mm/year. This suggests that there is high passivation on the surface of Ni-10Fe-40Co alloy compared to Ni-15Fe-35Co.

Heat-treated alloys showed a protective film on their surface except for Ni-10Fe-40Co (Fig. 14C) in which intergranular corrosion was observed. Intergranular corrosion may have been induced by hydrogen embrittlement which aids in the deformation causing a brittle fracture [37]. Materials of higher strength, are more susceptible to this type of fracture as they have smaller plastic zones, making them more prone to brittle failure [40]. However, there is a

Fig. 14 SEM images of corroded as-sintered (c) Ni-10Fe-40Co and (d) Ni-5Fe-45Co, and heat-treated (C) Ni-10Fe-40Co and (D) Ni-5Fe-45Co

black substance observed on the surface of Ni-20Fe-30Co (Fig 13A) which could be what initiated an attack on the passivation layer or just impurities. This agrees with the high corrosion rate recorded for Ni-20Fe-30Co (Table 3). Low corrosion rate recorded for Ni-15Fe-35Co and Ni-5Fe-45Co corroborates the findings in Figs 13B and 14D, respectively. However, the lowest corrosion rates for both sintered and heated-treated were recorded for Ni-5Fe-45Co alloy. This depicts that Ni-5Fe-45Co is more resistant to corrosion.

4 Conclusion

This paper investigated the effect of Co and Fe contents on the microstructure and corrosion behaviour of the Ni-Fe-Co superalloys immersed in a 3.5 wt% aqueous solution. From the experiments, the results can be summarised as follows.

1. Microstructures of the alloys showed a near-lamellar morphology which mainly consisted of coherent ($\gamma\prime$)-FeNi$_3$ and γ-(NiFe) precipitate phases. Heat-treating the sintered alloys promoted dissolution of Co-Fe (bcc) and Fe$_3$C phases in high Co content alloys. The relative density of the alloys increased with increasing Co content.

2. Corrosion resistance of the alloys improved with increasing Co and decreasing Fe content. Upon heat treating at 1000 °C, the overall corrosion rate of the alloys increased owing to the grain refinement and dissolution of $\gamma\prime$ precipitates. Heat treatment also improved the relative density of the alloys.

3. Alloys with low Co content showed the occurrence of pitting corrosion which indicated a preferential breakdown of the passive film due to presence of high amounts of Fe-containing precipitates that accelerated the corrosion rates. Improvement in corrosion resistance of heat-treated alloys may be attributed to the coating process of NiFe, FeNi$_3$ and FeCo precipitates by passive films containing γ(Ni,Fe) and γ(Co,Fe) phases.

Author contribution I.M.C. Bopape: investigations and draft manuscript. E.N. Ogunmuyiwa: supervision. M.B. Shongwe: supervision. N.P. Mphasha: manuscript editing and additional data interpretation. N.Ntholeng: manuscript editing and additional data interpretation.

Declarations

Ethics approval All authors confirm that they follow all ethical guidelines.

Consent to participate The authors declare that they consent to participate in this paper.

Conflict of Interest The authors declare no competing interests.

References

1. Geddes B, Leon H, Huang X (2010) Superalloys: alloying and performance. Asm International
2. Retima M, Bouyegh S, Chadli H (2011) Effect of the heat treatment on the microstructural evolution of the nickel based superalloy. Metalurgija 17:71–77
3. El-Bagoury N, Amin MA, Mohsen Q (2011) Effect of various heat treatment conditions on microstructure, mechanical properties and corrosion behavior of ni base superalloys. Int J Electrochem Sci 6(12):6718–6732
4. Mishra A, Shoesmith D (2014) Effect of alloying elements on crevice corrosion inhibition of nickel-chromium-molybdenum-tungsten alloys under aggressive conditions: an electrochemical study. Corrosion 70(7):721–730. https://doi.org/10.5006/1170
5. Zhao S, Xie X, Smith GD, Patel SJ (2005) The corrosion of inconel alloy 740 in simulated environments for pulverized coal-fired boiler. Mater Chem Phys 90(2-3):275–281. https://doi.org/10.1016/j.matchemphys.2004.04.006
6. Lu J, Huang J, Yang Z, Zhou Y, Dang Y, Zhao X, Yuan Y (2018) Effect of cobalt content on the oxidation and corrosion behavior of ni–fe-based superalloy for ultra-supercritical boiler applications. Oxid Met 89(1):197–209. https://doi.org/10.1007/s11085-017-9783-8
7. Frankel GS (1998) Pitting corrosion of metals: a review of the critical factors. J Electrochem Soc 145(6):2186–2198. https://doi.org/10.1149/1.1838615
8. Jang H, Park C, Kwon H (2005) Photoelectrochemical analysis on the passive film formed on ni in ph 8.5 buffer solution. Electrochim Acta 50(16-17):3503–3508
9. Magnussen O, Scherer J, Ocko B, Behm R (2000) In situ x-ray scattering study of the passive film on ni (111) in sulfuric acid solution. J Phys Chem B 104(6):1222–1226
10. Sarosi P, Wang B, Simmons J, Wang Y, Mills M (2007) Formation of multimodal size distributions of $\gamma\prime$ in a nickel-base superalloy during interrupted continuous cooling. Scr Mater 57(8):767–770. https://doi.org/10.1016/j.scriptamat.2007.06.014
11. Aba-Perea P, Pirling T, Withers P, Kelleher J, Kabra S, Preuss M (2016) Determination of the high temperature elastic properties and diffraction elastic constants of ni-base superalloys. Mater Des 89:856–863. https://doi.org/10.1016/j.matdes.2015.09.152. https://www.sciencedirect.com/science/article/pii/S026412751530561X
12. Zhao X, Dang Y, Yin H, Lu J, Yuan Y, Yang Z, Yan J, Gu Y (2016) Effect of heat treatment on the microstructure of a ni–fe based superalloy for advanced ultra-supercritical power plant applications. Prog Nat Sci: Mater Int 26(2):204–209. https://doi.org/10.1016/j.pnsc.2016.03.013. https://www.sciencedirect.com/science/article/pii/S1002007116300132
13. Zhong Z, Gu Y, Yuan Y, Shi Z (2014) Tensile properties and deformation characteristics of a ni-fe-base superalloy for steam boiler applications. Metall Mater Trans A 45(1):343–350
14. Pike L (2008) Development of a fabricable gamma-prime ($\gamma\prime$) strengthened superalloy. Superalloys 2008 191–200. https://doi.org/10.7449/2008/Superalloys_2008_191_200
15. Balikci E, Raman A, Mirshams R (1997) Influence of various heat treatments on the microstructure of polycrystalline in738lc. Metall Mater Trans A 28(10):1993–2003. https://doi.org/10.1007/s11661-997-0156-9
16. Collins D, Conduit B, Stone H, Hardy M, Conduit G, Mitchell R (2013) Grain growth behaviour during near-$\gamma\prime$ solvus thermal exposures in a polycrystalline nickel-base superalloy. Acta Materialia 61(9):3378–3391
17. Bopape I, Shongwe M, Ogunmuyiwa EN, Rominiyi A, Jeje S (2019) Influence of heat treatment on microstructure and mechanical properties of ni-fe-co ternary alloy prepared via spark plasma sintering. In: IOP conference series: Materials science and engineering, vol 655. IOP Publishing, p 012030. https://doi.org/10.1088/1757-899x/655/1/012030
18. Karimbeigi A, Zakeri A, Sadighzadeh A (2013) Effect of composition and milling time on the synthesis of nanostructured ni-cu alloys by mechanical alloying method. Iran J Mater Sci Eng 10(3):27–31
19. Rominiyi A, Shongwe M, Babalola B (2018) Development and characterization of nanocrystalline cobalt powder prepared via high energy ball milling process. In: IOP conference series: Materials science and engineering, vol 430. IOP Publishing, p 012029
20. Cam G, Koçak M (1998) Progress in joining of advanced materials part 2: Joining of metal matrix composites and joining of other advanced materials. Sci Technol Weld Join 3(4):159–175
21. Joseph C, Persson C, Colliander MH (2017) Influence of heat treatment on the microstructure and tensile properties of ni-base superalloy haynes 282. Mater Sci Eng: A 679:520–530
22. Oh JH, Choi IC, Kim YJ, Yoo BG, Ji Jang (2011) Variations in overall-and phase-hardness of a new ni-based superalloy during isothermal aging. Mater Sci Eng: A 528(19-20):6121–6127
23. Ganji DK, Rajyalakshmi G (2020) Influence of alloying compositions on the properties of nickel-based superalloys: a review. Recent Adv Mech Eng, 537–555
24. Turchanin M, Dreval L, Abdulov A, Agraval P (2011) Mixing enthalpies of liquid alloys and thermodynamic assessment of the cu–fe–co system. Powder Metall Met Ceram 50(1):98–116
25. Long H, Mao S, Liu Y, Zhang Z, Han X (2018) Microstructural and compositional design of ni-based single crystalline superalloys–a review. J Alloys Compd 743:203–220

26. Reed RC (2008) The superalloys: fundamentals and applications. Cambridge University Press, Cambridge

27. Hazotte A, Grosdidier T, Denis S (1996) γ' precipitate splitting in nickel-based superalloys: a 3-d finite element analysis. Scripta materialia 34(4):601–608. https://doi.org/10.1016/1359-6462(95)00554-4

28. Zhong Z, Gu Y, Yuan Y, Shi Z (2013) A new wrought ni–fe-base superalloy for advanced ultra-supercritical power plant applications beyond 700° c. Mater Lett 109:38–41

29. Çam G, Koçak M (1998) Progress in joining of advanced materials. Int Mater Rev 43(1):1–44

30. Berthod P (2019) Microstructures and metallographic characterization of superalloys. J Mater Sci Technol Res 6:39–52

31. Dutta R, Dey G (2003) Effects of partial crystallinity and quenched-in defects on corrosion of a rapidly solidified ti-cu alloy. Bull Mater Sci 26(5):477–482

32. Peters H Jr (2002) Natural surface phenomena and the impact of corrosion inducing salts. In: SSPC 2002 annual conference paper

33. Solomon I, Solomon N (2010) Effect of cobalt on the corrosion behavior of amorphous fe-co-cr-b-si alloys in dilute mineral acids. J Metall 46(5):389–395. https://doi.org/10.1179/cmq.2010.49.3.319

34. Leffler B (1996) Stainless steels and their properties. 2nd Ed. ISBN:91- 9720-216-9

35. Angelini E, Antonione C, Baricco M, Bianco P, Rosalbino F, Zucchi F (1993) Corrosion behaviour of fe80-xcoxb10si10 metallic glasses in sulphate and chloride media. Mater Corros 44(3):98–106

36. Altube A, Pierna A (2004) Thermal and electrochemical properties of cobalt containing finemet type alloys. Electrochimica Acta 49(2):303–311

37. Keogh MM (2019) Localised Corrosion of Ni-base Superalloys in Seawater. The University of Manchester (United Kingdom)

38. Ibrahim MF (2013) Effect of different sodium chloride (nacl) concentration on corrosion of coated steel. PhD thesis, UMP

39. Shongwe MB, Makena IM, Ajibola OO, Olubambi PA, Adams FV (2018) Effects of ternary metal additions on corrosion of spark plasma sintered ni-fe alloys in h2so4 and nacl. Bull Chem Soc Ethiop 32(2):337–349. https://doi.org/10.1080/02726351.2017.1298686

40. Beachem C (1972) A new model for hydrogen-assisted cracking hydrogen "embrittlement". Metall Trans 3(2):441–455